INVESTIGATIONS ON AMBIGUTY UNWRAPPING OF RANGE IMAGES

B. Jutzi

Institute of Photogrammetry and Remote Sensing, Universität Karlsruhe
Kaiserstr. 12, 76128 Karlsruhe, Germany
boris.jutzi@ipf.uni-karlsruhe.de

KEY WORDS: Range imaging, RIM, ambiguous, phase-unwrapping, modulation frequency, close range.

ABSTRACT:
For the first time the basic principle to unify advantages between active sensors and the simultaneous capturing of an image for an extended area of dynamical 3D applications in close range is given by range imaging (RIM) sensors. The drawback of data which is captured with RIM sensors is the absolute range accuracy and the limited non-ambiguity range. From other sensor systems different techniques are known to solve this problem in order to obtain a non-ambiguity range, e.g. by utilizing different modulation frequencies as most continuous-wave (CW) modulated laser scanner and radar systems do or by (pseudo) random modulation. In this paper a post-processing task is presented. The Goldstein 2D unwrapping procedure for unwrapping the range ambiguities of ranging sensors (e.g. RIM sensors or CW-modulated laser scanners) is proposed considering residues, branch cuts and tree estimation strategies and additionally confidence criteria. It could be shown that a range restoration for numerous periods of the ambiguity range is in principle possible with the presented 2D unwrapping procedure.

1. INTRODUCTION

Currently the geometrical 3D capturing and description of the environment are based on image or range data. By utilizing passive imaging sensors the 3D information is gained by textured image data indirectly from several images with costly stereo- or multiple image analysis. These procedures are widely used, but have indispensable claims due to capturing disposition and scene contents. For instance the illumination conditions should be adequate, the observed materials should be textured and opaque, and the distance between object and camera as well as between the camera viewpoints of stereo images should be sufficient large enough for gaining a reliable 3D reconstruction.

Beside this the photogrammetric methods are complemented by laser scanner procedures. These active sensors capture a sequence of singular range values while accomplishing a time dependent spatial scanning of the environment. Beside these basic range measurements the current commercial airborne laser scanner (ALS) developments allow to record the amplitude or the waveform of the backscattered laser pulse (Jutzi & Stilla, 2006). Therefore, laser scanner systems like OPTECH ALTM 3100, TOPEYE MK II, and TOPOSYS HARRIER 56 can be used. The latter system is based on the RIEGL LMS-Q560. More and more waveform capturing scanners are available at the moment, e.g. RIEGL - one of the leading companies for laser scanners - already offers several scanners (LMS-Q560, LMS-Q680, and VQ-480). In general spaceborne, airborne as well as terrestrial laser scanner sensors allow a direct and illumination-independent measurement of 3d objects (Shan & Toth, 2008).

For an accurate data acquisition necessarily the scene contents as well as the sensor platform should be static, otherwise a deformation of the environment can appear. In general with an increasing dynamic of the scene contents respectively sensor platform the complexity of the analysis increases and the exploitation of 3D information is more and more challenging. To gain three-dimensional information from rapid dynamical processes the capturing of the environment at the same time is essential. Very recently enhanced types of active imaging sensors have started to meet these requirements, namely the Swiss Ranger (www.mesa-imaging.ch), the PMD Vision (www.pmdtec.com), and the O3D series (www.ifm.de). These close range sensors (Table 1) allow to capture an range image and a co-registered intensity image simultaneously with high repetition rate (up to 100 releases per second). The non-ambiguity range is currently below 7.5m and depends on the modulation frequency. The measured intensity strongly depends on the used wavelength (usually close infrared) of the laser source and the surface characteristic.

For the first time the basic principle to unify advantages of active sensors and the simultaneous capturing of an image for an extended area of dynamical 3D applications is given. Especially the 3D monitoring in close range with airborne and terrestrial platforms in problematic weather and illumination conditions or at night is promising with this novel technology. Therefore different applications are building surveillance, traffic monitoring, and driver assistance. Beside this, the 3D motion or deformation analysis, like autonomous navigation of robots, trajectory tracking of pedestrians for surveying, or maker free 3D measurements of crash tests, are of interest.

Another technical advantage is the monostatic sensor configuration, which allows to observe the area of interest from a single point of view, in contrast to the classical stereo observation techniques with passive sensors, which need at least two different viewpoints. The mayor drawbacks are the limited non-ambiguity range and the absolute range accuracy of a few centimeters. Especially the relatively large noise influence on the measurement, due to the large amount of ambient radiation in comparison to the emitted radiation, results in a range measurement which is less reliable compared to the performance of airborne or terrestrial laser scanner (TLS). However concerning the technical progress, most limitations will be overcome soon and in close future systems with expanded operating range and improved image size will be available.

The terminology for scannerless range imaging systems is multifarious, the terms Time-of-Flight (TOF) depth camera, 3D range imager, Time-of-Flight Sensors, photonic mixer devices (PMD; Schwarte, 1997), or often a combination of the mentioned terms are used. Unfortunately, most of the terms are much more related to the range measurement than on the as well available gray value measurement of the observed area. For the procedure the term range imaging with the abbreviation RIM is more and more established, especially in Europe.

Various studies about range imaging have been published in the literature dealing with different interests. Beside the hardware and sensor developments (Lange, 2000), nowadays most works focus on geometric and radiometric calibration:

- Reulke (2006) introduced a geometrical calibration and fused the intensity image derived by the range imaging sensor with high resolution RGB data to improve the texturing of surfaces.
- Kahlmann et al. (2007) focused on the geometric calibration of range imaging sensors and developed a tracking of moving objects (people) approach based on recursive Bayesian filter.
- Lichti (2008) proposed a method for the self-calibration by bundle adjustment of range imaging sensors which allows a simultaneous calibration concerning the spatial distortions and the ranging system.

Other works focused on tracking of objects and automatic extraction of object features:

- For the tracking of human motion and interaction within a range image sequence, Westfeld & Hempel (2008) suggested the combination of complementary radiometric and geometric information to increase accuracy and reliability.
- For a moving range imaging Karel et al. (2007) specified an automatic object segmentation sensor based on a fast minimum covariance determinant approach and evaluated statistically the quality of the data.
- Kim et al. (2008) proposed to utilize more than one synchronized range imaging system to gain multi views for the reconstruction of dynamic scenes.

As briefly mentioned above one drawback of the RIM sensors is the limited non-ambiguity range. From other sensor systems different techniques are known to solve this problem in order to obtain a non-ambiguity range, e.g. by utilizing different modulation frequencies as most continuous-wave (CW) modulated laser scanner and radar systems do or by (pseudo) random modulation.

In this paper a post-processing task is investigated in contrast to the above mentioned and not yet for RIM sensors available technical improvements. It has to be mentioned that the ambiguous range subject is close related to the well known phase unwrapping problem which is extensively discussed in the radar interferometry community. This inverse problem cannot be solved in general and intensive research is going on this issue until today. For instance one large drawback is the sensitivity of the phase reconstruction to minor measurement errors. Additionally, the reconstruction suffers from multiple integer solutions caused by the unwrapping procedure. Usually the measured environment is unknown and, therefore, multiple integer solutions are possible, if the topography contains large geometrical discontinuities.

In this paper a method for unwrapping the range ambiguities of range imaging sensors is proposed. In Section 2 the measurement principle of range imaging sensors, a 1D straight forward and the Goldstein 2D unwrapping procedure are introduced. In Section 3 the sensor and scene configuration is presented and in Section 4 the data are examined. The analysis by the mentioned unwrapping procedures is described in Section 5 considering residues, branch cuts and tree estimation strategies, and the confidence criteria. Finally, the derived results are evaluated and discussed, the content of the entire paper is concluded, and an outlook is given.

2. METHODOLOGY

2.1 Measurement principle

The range measurement can be briefly described as follows: First a sinusoidal CW modulated signal is transmitted by a LED array in form of monochromatic light. The emitted light travels to the object, is backscattered by the illuminated surface, and captured by a receiver array (usually CCD or CMOS arrays). Concerning a demodulation of the sinusoidal received signal the parameters amplitude A and phase φ can be determined. For each measurement four neighborhood pixels are utilized to measure the four received intensities with a relative phase shift of 90°, or with other words an absolute phase shift of 0°, 90°, 180°, and 270°. Then the phase shift $\Delta\varphi$ between the transmitted and received signal can be determined by the intensity values A_0, A_{90}, A_{180}, and A_{270}, with

$$\Delta\varphi = \arctan\left(\frac{A_{270} - A_{90}}{A_0 - A_{180}}\right). \quad (1)$$

Based on the phase shift $\Delta\varphi$ the range R to the object is given with respect to the two-way time of flight by

$$R = \frac{c}{2 f_m}\frac{\Delta\varphi}{2\pi}, \quad (2)$$

where f_m is the modulation frequency and c the speed of light.

2.2 Data characteristic & feature convention

The range ambiguity ΔR can be denoted by

	MESA Swiss Ranger		PMD [Vision]		
Type	**SR-3000**	**SR-4000**	**O3**[a]	**S3**[a]	**CamCube 2.0**
URL	www.mesa-imaging.ch		www.pmdtec.com		
Image size	176x144	176x144	64x48	64x48	204x204
Focal length [mm]	8	10	TBD	-	12.8
Field of View (FoV) [°]	47.5x39.6	43.6x34.6	40x30	40x30	40x40
Pixel size [µm]	40x40	40x40	100x100	100x100	TBD
Wavelength [nm]	850	850	850	850	870
Power (optical) [W]	≤1	≤1	ca. 1	ca. 4	TBD
Frame rate [1/s]	max. 15-20	max. 54	max. 25	max. 20	max. 25
Modulation frequency [MHz]	20	29, 30, 31	20	20	variable
Non-ambiguity range [m]	7.5	5	7.5	7.5	7.5
Size [mm]	60x50x65	65x65x68	60x42x54	120x75x95	60x187x60
Outdoor feasibility	no	yes[b]	yes[b]	yes[b]	yes[b]

Table 1. Specification overview of selected range imaging sensors: MESA Swiss Ranger series (www.mesa-imaging.ch) and PMD Vision series (www.pmdtec.com). URLs accessed on June 2009.
[a] PMD [Vision] O3/S3 are equivalent to IFM (www.ifm.de) O3D100/ O3D200, [b]Suppression of background illumination.

$$\Delta R = \frac{c}{2 f_m} . \quad (3)$$

To estimate the absolute range R for the ambiguity an integer k is multiplied with the range ambiguity ΔR

$$R = \Delta R k . \quad (4)$$

To resolve the range ambiguity various methods are known in literature. A general overview of the existing methods is given in Ghiglia & Pritt (1998). Most of these approaches deal with 2D data sets. In contrast to this, the capturing of a scene with a RIM system delivers a 3D data set composed out of voxels with two spatial coordinates *x,y* and one time coordinate *t*

$$Q(x, y, t) , \quad (5)$$

where for each voxel different features are measured, e.g. *range R, intensity I,* and *confidence-of-the-measurement C*. Then for each feature a single data cube is given by Q_R, Q_I, and Q_C.

In the following, a stationary sensor setup is assumed for observing a high dynamical temporal and spatial scene. Two methods were examined and a brief overview is given in the following Sections.

2.3 1D straight forward unwrapping

With this straight forward approach a separability of the data set is assumed based on a sequential accomplished 1D unwrapping. Additionally, a mask, which is available from the data cube Q_C with the feature *confidence-of-the-measurement*, can be used to mask out unreliable voxels.

The drawback of this approach is that only a single voxel in the neighborhood of the six connected voxels (joint faces connection) is considered and the result depends on the processing direction and order. Therefore the topology is principally ignored and due to this, the 1D processing causes an erroneous unwrapping which results in a striped pattern. This inadequate approach was implemented mainly for comparison purposes and to visualize the problematic of ambiguity range unwrapping.

2.4 Goldstein 2D unwrapping

The Goldstein approach is described in detail in various publications, e.g. Goldstein et al. 1988. Originally it was developed for phase unwrapping in radar interferometry. The suggested solutions to reconstruct the unknown phase can be analogue transferred to the ambiguous range problematic. A brief description of unwrapping the ambiguous range will be given in this section.

The goal of unwrapping is to find integers k which can be added to the measured values to gain a continuous representation. The measured values are within a cycle of zero and the non-ambiguity value. In general phase unwrapping approaches are based on processing the changes between the pixels or respective voxels in the direct neighborhood by gradient calculation. Then the values are integrated by predefined rules and finally, if a discontinuity is detected, the most likelihood integer solution for unwrapping is added. To get a reasonable solution it is essential to find an optimal integration path for the gradient.

The unwrapping procedure is highly over determined. Therefore, different constraints have to be assumed. The key assumption is moderate changes within the neighborhood with relative changes below the ambiguity value. Values above are called discontinuities and have to be bypassed by the restoration procedure. The discontinuities can be reduced to inconsistencies within the range values, so-called residues. Residues are given if the sum of four neighborhood pixels calculated in circular direction is unequal to zero. This procedure is path dependent and further it is very sensitive to noise.

The identified residues are connected to generate so-called branch cuts. Usually the length of the branch cuts (distance between the residues) should be as short as possible. The idea behind the branch cut is to find close by negative and positive residues (sometimes called dipoles) which can be compensate by each other if the total charge along the branch cut is zero. If the total charge is nonzero, the search continues for additional close by residues. Each associated residue is connected to the tree by means of a branch cut and the total charge is calculated. If the total charge is zero the tree is considered. The disadvantage of this procedure is that coordinates (position) of the branch cuts are arbitrarily chosen leaving out important context information. A better solution might be to utilize a more expensive approach, like for instance the Mask-cut-algorithm, which take into account the quality concerning the position of the selected cuts.

For the continuative search of associated residues, regardless if the residues have been previously assigned, they are added to a new tree. This results in a dendritic form of the branch cuts. Finally, the derived tree has to be bypassed for the integration calculation to utilize the unwrapping procedure.

This procedure can be additionally supported by the *confidence-of-the-measurement* to mask out unreliable range values.

3. CONFIGURATION

3.1 Sensor

For the investigations a Swiss Ranger SR-4000 sensor was used with the specifications listed in Table 1. The sensor has a 176 x 144 pixel array with a pixel size and pitch (spacing) of about 40 µm. The user can preselect the modulation frequency with 29, 30, and 31 MHz, which results in a maximum non-ambiguity range of 5.17, 5.00, and 4.84 m. The maximum frame rate is about 50 frames per second. Therefore, the number of 3D points measured by a range imaging system is above one million points per second which is equivalent to the current point capturing rate of the fastest close range laser scanners.

3.2 Scene

A range image sequence of an indoor scene was recorded by a stationary placed sensor. 100 frames were captured with a frame rate of 12 frames per second while the person was moving in direction to the sensor within a furnished room. A single RGB image of the observed scene is depicted in Figure 1. For the environment no reference data concerning the radiometry or geometry were available.

Figure 1. RGB image of the observed indoor scene.

4. DATA EXAMINATION

To depict the neighborhood relations of the feature *range*, the data cube was sliced in different directions: equivalent to the captured frames in *y-x* slices, vertically in *t-y* slices, and horizontally in *x-t* slices. The same procedure was done for the feature *intensity*. Figure 2 shows a set of images for the different slices in the space-space and space-time domain with the corresponding range and intensity images. The images have been normalized for visualization purposes and range and intensity values are depicted as gray values.

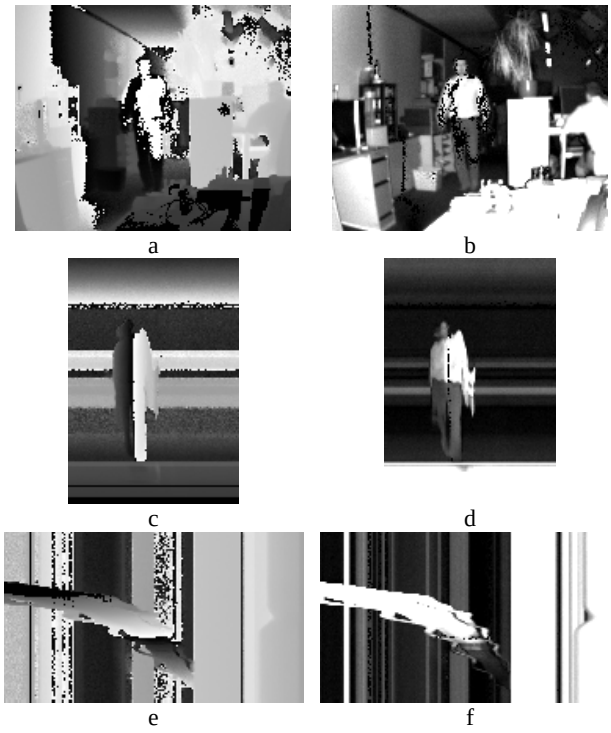

Figure 2. Corresponding *range* and *intensity* images differently orientated: a&b) *x-y*, c&d) *t-y*, and e&f) *x-t* slice.

For the measurements a modulation frequency of 29 MHz was selected which results in a range ambiguity of ΔR=5.17 m. The range ambiguity is below the extension of the room. Figure 2a obviously shows several range ambiguity crossings. The discontinuities of the gray values can be seen by comparing them with the continuous appearance of the gray values of the intensity in Figure 2b, e.g. on the plan wall on left side. Further the range and slope dependent measured intensity values, which decrease with increasing range, are noticeable on the wall and on the ceiling. The intensity I can be normalized by the corresponding range r with

$$I \propto \frac{1}{r^2}. \qquad (6)$$

Due to the stationary sensor setup the *t-y* and *x-t* slices contain mainly a stripy pattern, which is typical for a static scene. This pattern is interrupted by a specific representation of the dynamic procedures within the scene, which can be recognized as motion area. In Figure 2c-f the moving person is visible, but the representation is obviously deformed. In Figure 2c&e within the motion area the black to white crossover of the regions shows an object (person) crossing the ambiguity range during the measurements.

Beside the feature *range* and *intensity* the *confidence-of-the-measurement* is available. In Figure 3a the quality of the measurement is coded by gray values, dark values for a low confidence (bad) and bright values for a high confidence (good). Obviously the measurements close to the ambiguity range appear with a bad signal-to-noise ratio and, therefore, the confidence is low. Furthermore, the quality of the measurement is range dependent, measurements in far range are less reliable than in close range. This can be observed for instance at the wall on the left side of the room. Further if the measured intensity is above the dynamic range, the receiver saturates and the measurement is unusable. The statistic of the quality for the investigated slice is depicted in Figure 3b. It can be seen that most of the measurements are reliable, but about 11% of the measurements are unreliable, where the *confidence-of-the-measurement* C is equivalent to 0.

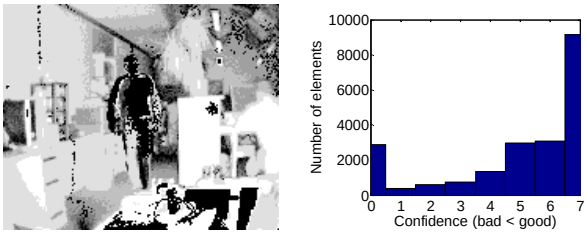

Figure 3. *Confidence-of-the-measurement* image (a) and corresponding histogram (b) for *x-y* slice.

5. ANALYSIS RESULTS

5.1 1D straight forward unwrapping

The 1D straight forward unwrapping does not take into account all neighborhood relations. An example for the unwrapping procedure is depicted, where in Figure 4a the original ambiguous range (dashed red line), the ambiguity range (dotted green line), and the 1D unwrapped range (solid blue line) are shown. Furthermore, the corresponding intensity values are presented in Figure 4b. Comparing the characteristic of the ambiguous range with the intensity values, the unreliability of the measured values is obvious (e.g. at pixel coordinate 25). At this range the intensity values are noisy compared to the nearby values. After unwrapping the dynamic range interval implies about four periods of the range ambiguity ΔR in the depicted example.

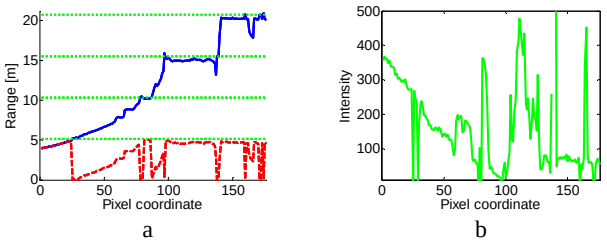

Figure 4. 1D examples for the characteristic of corresponding range and intensity values of a single row: a) Original ambiguous range (dashed red line), ambiguity range (dotted green line), and 1D unwrapped range (solid blue line), b) intensity (solid green line).

Utilizing this approach on the *x-y* slices it can be shown that the derived results depend on the unwrapping direction due to the discontinuities of the range values. In Figure 5 the results for different processing directions are presented. Most of the

failures are induced by unreliable measurements, which will be demonstrated in the following Section.

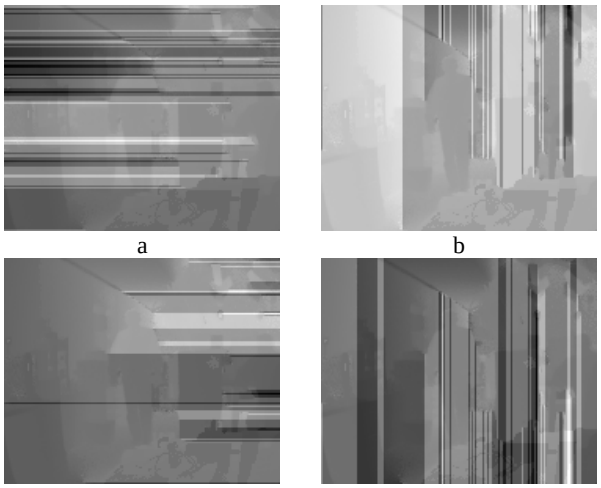

a b c d

Figure 5. 1D straight forward unwrapping results for different processing directions: a) Right to left, b) bottom to top, c) left to right, d) top to bottom.

5.2 Residues, branch cuts and tree estimation

First, all residues are calculated for all *x-y* slices of the data cube Q_R. In Figure 6a the negative and positive residues (black and white colored pixels) for the *x-y* slice in Figure 2a are depicted. All in all 64 residues were determined. To proof the reliability of the residues for each residue the corresponding *confidence-of-the-measurement* voxel is extracted. A histogram with the statistic for the reliability of all residues is depicted in Figure 6b. It clearly shows that most of the determined residues base on an unreliable measurement, as 26 residues have the *confidence-of-the-measurement* 0 and, therefore, they are unreliable. This coincides with the already mentioned statement that the procedure to calculate residues is very sensitive to noise.

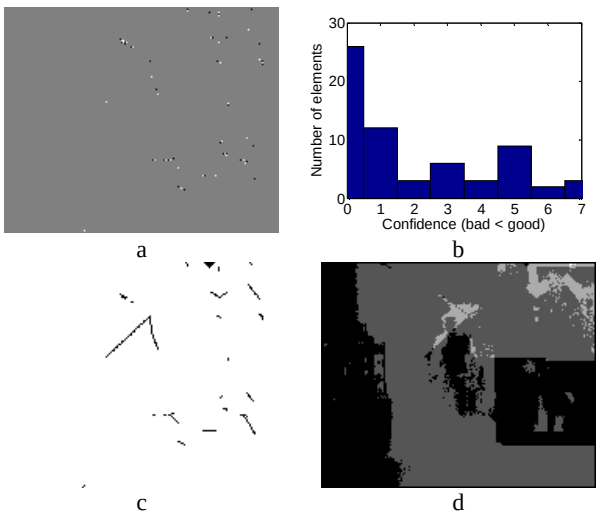

a b c d

Figure 6. Intermediate results: a) Extracted residues, b) reliability of the residues, c) branch cuts and trees, d) number of gained range offsets ΔR.

In Figure 6c all connected residues in form of branch cuts are shown, where all branch cuts are linked together to the final trees. For the following integration procedure to unwrap the range areas it is interdicted to cross the branch cuts. The number of gained range offsets ΔR coded by integer values are depicted in Figure 6d. For the black areas the number is zero, this denotes the original range is already non-ambiguous. The gray areas show that ambiguous range areas have been detected and solutions up to a range ambiguity of four periods (bright gray areas) could be determined.

Concerning the residues on the afore mentioned 1D straight forward unwrapping approach in Section 5.1 it can be easily shown with Figure 7 that the remaining discontinuities derived by the erroneous range unwrapping have their origin at the coordinates of the residues (black pixel).

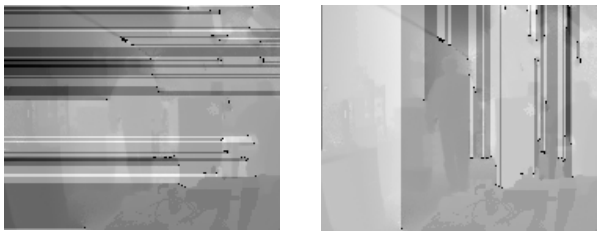

a b

Figure 7. Visualization of residues (black pixel) and 1D straight forward unwrapping results of Figure 5a&b.

5.3 Goldman 2D unwrapping concerning the confidence criteria

The given data cube Q_C (*confidence-of-the-measurement*) provides information about the quality of the measurement, where the ranking of the quality is within the interval 0-7 and the values start from unreliable (value 0) up to excellent (value 7). A histogram for a single *x-y* slice is shown in Figure 3.

In the following the quality of the measurement on the reconstruction of the absolute range is investigated. Therefore, different tests were carried out to verify the influence of the quality of the measurement on the reconstruction of the absolute range. Overall seven tests were carried out by utilizing the confidence masks to verify the influence of the quality of the measurement on the reconstruction for the absolute range by the 2D unwrapping process. Only the reliable ambiguity range values above a given threshold are considered for processing. According to this the low quality measurements have been rejected.

Selected results are depicted in Figure 8. In close range, below two periods of the ambiguity range and with modest discontinuities the range unwrapping is reliable (e.g. the wall on the left side). Erroneous range unwrapping can be observed in all four results, where most of the wrong unwrapping range values appear at far range, above two periods of the ambiguity range. At this range the data quality is poor and the range values might be noisy. In addition to this, numerous discontinuities are at this range. Furthermore, it has to be mention that the results mainly depend on the seed point initialization and on the connectivity of the segments.

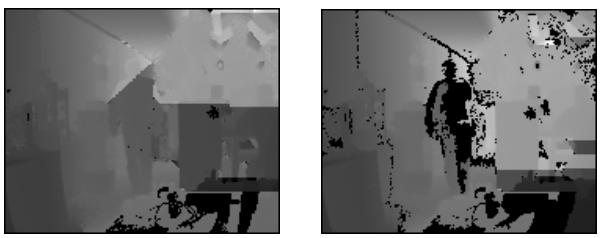

a b

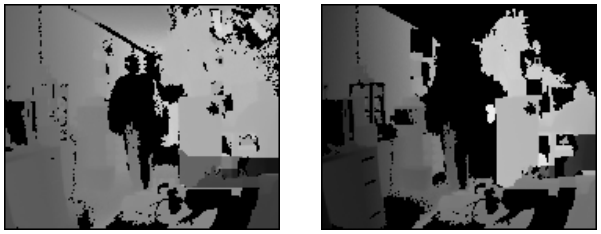

c d

Figure 8. Unwrapping results considering confidence masks: a) Interval 0-7 (equivalent to all data processing), b) interval 2-7, c) interval 4-7, and d) interval 6-7.

5.4 Range dependent intensity normalization

Finally, the range dependent correction of the measured intensity is calculated by utilizing Formula 4. The measured intensity (Figure 2b) can be compared with the range corrected intensity (Figure 9a). The derived intensity for the same material (e.g. wall on the left) is equalized over the complete range area. Of a selected 1D example (dotted white line in Figure 9a) the corresponding intensity values (solid blue line) are depicted in Figure 9b. For comparison purposes the measured intensity (solid green line) and the unwrapped range corrected intensity (dashed red line) is shown. Still some artifacts are remaining from unreliable pixels at the 1D example and within the intensity image (e.g. at the person).

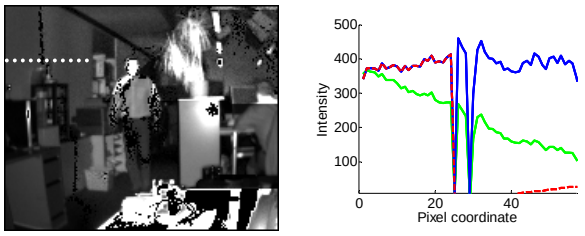

a b

Figure 9. Range corrected intensity. a) Image, b) 1D example.

6. EVALUATION AND DISCUSSION

The evaluation of the results is difficult because geometric and radiometric reference data are not available. Therefore, the evaluation was performed by visual criteria. It could be observed that the range unwrapping sometimes fails, where most of the wrong range values appear at far range, above two periods of the ambiguity range, because at this range the data quality is poor and the range values might be noisy. However, in general an improvement could be gained.

Obviously the main disadvantage of the Goldman 2D unwrapping approach is the way the branch cuts are determined because they were selected by the criteria to be as short as possible (Figure 6c) and they do not rely on topographical aspects. This should be improved by more expensive approaches, like e.g. the Mask-cut-algorithm, which take into account the quality concerning the position of the selected cuts. In general the reconstruction suffers from multiple integer solutions if the topography contains large geometrical discontinuities.

By considering the confidence-of-the-measurement the result could be further improved, but in this case it is always a trade of between incomplete and erroneous results.

7. CONCLUSION AND OUTLOOK

It could be shown that a range restoration for numerous periods of the ambiguity range is in principle possible with the presented 2D unwrapping procedures. For future work the confidence-of-the-measurement might be a reliable basis for a quality guided unwrapping approach. Furthermore, due to the availability of a 3D data set, a 3D unwrapping procedure might be promising. Beside these approaches which mainly base on a single sensor system, the utilization of more than one synchronized range imaging system to gain multi views might be of interest to solve the range unwrapping problem.

ACKNOWLEDGEMENT

The author would like to thank the members of MESA Imaging for assistance during the measurements.

REFERENCES

Ghiglia, D. C., Pritt, M. D., 1998. Two-Dimensional Phase Unwrapping: Theory, Algorithms, and Software. John Wiley & Sons: New York.

Goldstein, R. M., Zebker, H. A. Werner, C. L., 1988. Satellite radar interferometry: two-dimensional phase unwrapping. Radio Science, 23, pp. 713-720.

Jutzi, B., Stilla, U., 2006. Range determination with waveform recording laser systems using a Wiener Filter. ISPRS Journal of Photogrammetry & Remote Sensing 61 (2): pp. 95-107. [doi:10.1016/j.isprsjprs.2006.09.001]

Kahlmann, T., Remondino, F., Guillaume, S., 2007. Range imaging technology: new developments and applications for people identification and tracking. In: Beraldin, J.-A., Remondino, F., Shortis, M. R. (Eds.) Videometrics IX, SPIE Proceedings Vol. 6491, 64910C.

Karel, W., Dorninger, P., Pfeifer, N., 2007. In Situ Determination Of Range Camera Quality Parameters By Segmentation. In: Gruen A, Kahmen H (Eds.) Optical 3-D Measurement Techniques VIII, pp. 109-116.

Kim, Y. M., Chan, D., Theobalt, C., Thrun, S., 2008. Design and calibration of a multi-view TOF sensor fusion system. In Proceedings of IEEE CVPR Workshop on Time-of-flight Computer Vision 23-28 June 2008, pp. 1-7.

Lange, R., 2000. 3D time-of-flight distance measurement with custom solid-state image sensors in CMOS/CCD-technology. PhD thesis, University of Siegen.

Lichti, D. D., 2008. Self-Calibration of a 3D Range Camera. International Archives of Photogrammetry, Remote Sensing and Spatial Geoinformation Sciences 37 (Part B5), pp. 927-932.

Reulke, R., 2006. Combination of distance data with high resolution images. In: Maas, H.-G., Schneider, D. (Eds.) ISPRS Commission V Symposium: Image Engineering and Vision Metrology, International Archives of Photogrammetry, Remote Sensing and Spatial Geoinformation Sciences 36 (Part B).

Schwarte, R., Xu, Z., Heinol, H.-G., Olk, J., Klein, R., Buxbaum, B., Fischer, H., Schulte, J., 1997. New electro-optical mixing and correlating sensor: facilities and applications of the photonic mixer device (PMD). In: Loffeld, O. (Ed.) 3D Sensors and 3D Imaging, SPIE Proceedings Vol. 3100, pp. 245-254.

Shan, J., Toth, C.K., (Eds.) 2008. Topographic Laser Ranging and Scanning: Principles and Processing. Boca Raton, FL: Taylor & Francis.

Westfeld, P., Hempel, R., 2008. Range Image Sequence Analysis by 2.5-D Least Squares Tracking with Variance Component Estimation and Robust Variance Covariance Matrix Estimation. International Archives of Photogrammetry, Remote Sensing and Spatial Geoinformation Sciences 37 (Part B5), pp. 933-938.